Hindawi
International Journal of Energy Research
Volume 2023, Article ID 9929496, 18 pages
https://doi.org/10.1155/2023/9929496

Research Article

Inverse Heat Transfer Analysis Method to Determine the Entropic Coefficient of Reversible Heat in Lithium-Ion Battery

Ukmin Han, Hongseok Choi, Hyoseong Lee, and Hoseong Lee

Department of Mechanical Engineering, Korea University, 409 Innovation Hall Bldg., Anam-Dong, Sungbuk-Gu, Seoul, Republic of Korea

Correspondence should be addressed to Hoseong Lee; hslee1@korea.ac.kr

Received 13 September 2022; Revised 9 November 2022; Accepted 10 November 2022; Published 3 February 2023

Academic Editor: Weiwei Han

Copyright © 2023 Ukmin Han et al. This is an open access article distributed under the Creative Commons Attribution License, which permits unrestricted use, distribution, and reproduction in any medium, provided the original work is properly cited.

An entropic coefficient of reversible entropic heat is a key parameter in determining the battery thermal responses, but its measurement is challenging due to time consuming and inaccurate traditional methods. In this regard, an analytical approach based on the inverse heat transfer problem is newly proposed to precisely determine the entropic coefficient with low experiment cost. Experiments are conducted by discharging the battery under four different current rates to inversely estimate the entropic coefficients, and the least squares regression are conducted to optimize the derived entropic coefficients. Through the comparison with the existing potentiometric method, the experimental time can be reduced by 93.7%. Furthermore, the accuracy of the proposed method is well verified by validating within the root mean square error of 0.848°C by comparing with the experimental results. Through the validation processes under various operating conditions, such as low to high current rates, charging process, dynamic loads, and different ambient temperatures, the proposed method is proven over temperatures ranging from 10°C to 60°C. Conclusively, the proposed method can be a great alternative to replace the classical experimental methods.

1. Introduction

For decades, lithium-ion batteries (LiBs) have been actively used as high-efficiency energy storage devices in various industries, from small portable electronic devices to medium-to-large energy storage systems for electric vehicles (EVs) or power grids. In general, the LiBs generate heat within the cell during charging or discharging, and the battery thermal responses become much more severe with the continuously increased capacity and power. Thus, the careless battery uses without the cooling system could rapidly increase its temperature, possibly inducing thermal degradation and accelerating the irreducible aging rate, reducing the total lifetime [1]. A variety of battery thermal management studies have been introduced to predict these thermal aging effects for ensuring the safe use of batteries. Representatively, precise SOH estimation methods for real EV applications [2] have received a lot of attention. Along with the development of cutting edge techniques based on machine learning, studies on predicting thermal state of the battery under normal conditions but also at extreme situations like thermal runaway are being introduced [3]. Above all, studies on the battery thermal management system (BTMS) have received a lot of attention that BTMSs using heat passive systems such as phase change material [4] and heat pipe [5], integrated with the classical active cooling systems, are being actively introduced. As such, a variety types of studies have been conducted on the performance and safe use of the battery system, and they are all closely related to the battery thermal behavior. For these reasons, the most important thing in designing a battery system is accurate analysis and understanding of the battery thermal behavior. Equally, it is necessary to develop a fast and accurate analytical method for battery heat sources in particular.

Thus far, numerous studies have been conducted on analyzing the battery heat generation during operation. According to the Bernardi equation [6] with the assumption of negligible mixing and phase change effects [7], the battery heat generation is primarily composed of two primary heat sources, the irreversible joule heat and reversible entropic

heat. The former is the exothermic heat due to the internal resistance caused by the current flows and the latter one owes to the entropy change (ΔS) between two active materials. Unlike the joule heat, the entropic heat could be both exothermic and endothermic depending on the sign of the entropy change. The entropy change can be replaced by the entropic coefficient ($\partial U_{oc}/\partial T$) through the thermodynamic relation [8], representing the temperature derivative of the open-circuit voltage (U_{oc}: OCV). Since the entropy change in the battery denotes the structural change between the cathode and anode during charge or discharge, they can be either positive or negative and so is the entropic coefficient. The entropic coefficient is generally differed by the operating conditions of the battery, such as the current rate (C-rate), which is the measure of the rate at which battery is charged or discharged with respect to its nominal capacity, environmental conditions temperature, and aging condition. In particular, it is highly dependent on the state of charge (SOC) of the battery. Therefore, it is relatively difficult to measure the entropic coefficient compared with measuring the internal resistance of the former joule heat. Taking into account that the internal resistances can be reduced or minimized via a suitable cell design, the entropic coefficient, which is the main thermal property of the LiB, can be a key player in determining the thermal behavior of the battery. Consequently, it is essential to analyze the entropic coefficients according to the battery SOC as precisely as possible.

Up till now, various methods have been conducted to obtain the entropic coefficient of the LiBs. They are fundamentally based on experimental methods but can be specifically divided into two categories, classical and modified experimental methods. Representatively, classical methods are the potentiometric method based on thermodynamic theory and the calorimetric method using the calorimeter [9]. They have been used for decades to measure the entropic coefficient of the LiBs, and recently, several modified experimental methods have been proposed to compensate for the shortcomings of the preceding methods. Their characteristics are as follows. First, the potentiometric method analyzes the relationship between the voltage and temperature by measuring the OCV of the battery while changing the temperature in a specific SOC of the battery. Then, they are determined by calculating the slope of the OCV versus temperature. Since the potentiometric method was first introduced by Thompson [10], it has been mostly adopted in many previous studies on battery thermal analysis. However, there is an unavoidable drawback of taking a huge relaxation time to meet the electrical-thermal equilibrium state. Another experimental method is the calorimetric method using calorimeters, accelerating rate calorimeter [11, 12], or isothermal heat conduction calorimeter [13, 14] to measure the battery heat generation rate during charging and discharging. The method derives the average entropic coefficients according to the battery SOC under the assumption that the same joule heat is generated during charging and discharging processes if the same C-rate is applied. Compared to the potentiometric method, the calorimetric method can save considerable time, but its inaccuracy is often pointed out, and there is a fatal disadvantage that the size of the battery is limited by the size of the equipment [15].

Recently, some new methodologies to strengthen or replace the above traditional methods have been introduced to measure the entropic coefficients of LiBs more accurately. Schmidt et al. measured the entropy change via electrothermal impedance spectroscopy by observing the temperature fluctuations of the LiBs by applying the sinusoidal current with a different frequency [16]. Osswald et al. introduced the advanced measurement protocol of classical experimental methods. They used the background correction approach to derive the entropy profiles of LiBs, reducing the measurement time from several weeks to a few days while not scarifying the measurement accuracy [17]. Damay et al. proposed the advanced calorimetric method along with the improvement plans of the existing calorimetric method. According to the authors, it is possible to accurately obtain entropy-variation as a function of SOC by creating experimental conditions of high cell temperatures and low current-rates [18]. Geifes et al. extracted the entropic heat coefficient from the pulse relaxation measurement and refined them through least squares estimation. The method seems to be similar to the previous potentiometric method but succeeded in saving the experimental cost [19]. From then on, the so-called methods used for data analysis, such as the time or frequency domain method, were used to derive the continuous entropic coefficients of the battery. Hu et al. proposed the new method for measuring entropic coefficients based on the hybridized time-frequency domain analysis technique. Although the method itself is similar to the existing method, they succeeded in deriving the entropic coefficients through the background correction from the time domain to the frequency domain [20]. Based on this, Hu and Choe continued to develop an improved calorimetric method with the wavelet transform technique. Their data processing was applied the method on the battery heat generation data resulting from the isothermal calorimeter, successfully improving the accuracy of the conventional calorimetric method [21]. Similarly, Abbasalinejad et al. used the frequency-domain method and modified it to couple with the physics-based electrochemical-thermal battery model. The model was used to fit the entropy of reaction and proved its feasibility by comparing it with traditional methods [22].

From the literature review, the classical experimental methods are found to require too much time or reveal low accuracy in estimating the entropic coefficients of the battery. In particular, the most used potentiometric method, which highly depends on the linear interpolation between intermittently measured values, cannot derive continuous entropic coefficients as a function of SOC. Therefore, it inevitably requires repetitive experimental processes at the closest SOC interval as possible to obtain accurate values, which increase the experimental time several times. The calorimetric method likewise suffers from a low accuracy problem from its unclear assumption. Despite some recently presented methods to substitute the above experimental methods, the following limitations remain clear; most of them tried improving existing experimental methods, but it

is recognized to yet require a considerable amount of experimental time. Above all, there are very few studies that verify the developed method in terms of battery temperatures during operation. One of the main purposes of measuring the entropic coefficient is to predict the battery thermal behavior precisely; thus, it is requisite to check whether the proposed method or newly obtained entropic coefficients are applicable under various charging and discharging conditions.

The limitation of previous studies is an excessive dependency on classical experimental methods, impeding the precise and fast measurement of the entropic coefficients. In this context, the current study develops a new analytical approach to estimate the entropic coefficients of the battery, aiming to reduce the measurement time while ensuring accuracy. An inverse heat transfer analysis (IHTA) method is used intending to make the entropic coefficients the only unknown parameter in the energy equation, and in this process, the numerical generalized reduced gradient (GRG) algorithm is mainly used to find out the optimal heat transfer coefficient of the battery. The IHTA method is then used to calculate the entropic coefficients continuously according to the battery SOC, and the newly obtained values are refined through the regression analysis and least squares estimations to achieve representative values. Through the comparison with the existing experimental method, the high precision and time-efficient attributes of the proposed IHTA method are verified. For the last, the validation under various operating conditions such the cases of low to high C-rates, charging process, dynamic load conditions, and different ambient temperatures is mainly conducted to prove the feasibility of the developed method in predicting the battery thermal behaviors. The main contribution of the current work is to develop the new analytical method that can obtain the entropic coefficients the with the utilization of the numerical technique and minimal experimentation. Especially, the proposed method is expected to be universally applied to any LiBs without repetitive processes of preexperiments for battery thermal analysis.

2. Research Approach

In most scientific problems, it is usual to solve the governing equations with given or defined boundary conditions (causes) to predict the results, and this process is called a forward problem. An inverse problem is an opposite case of the forward problem, and it is named as an inverse heat transfer problem when applying to thermal analysis. Inverse heat transfer problems are often used to estimate the unknown parameters in the mathematical formulation of physical processes in thermal sciences by using the measured data, such as temperature, from the experiment [23]. It has been applied to various types of heat transfer analysis in previous literature with analytical or numerical methods, usually obtaining the thermal properties of the material: thermal conductivity and convective heat transfer coefficient. Focusing on that, the entropic coefficient (EC) is similarly a unique physical property of each LiBs since it is commonly a function of SOC [24]; it is possible to inversely derive the value of EC by solving the inverse heat transfer problems. From this point of view, the current study has tried to find the ECs by building the analytical solutions of the energy equation for the battery cell from the boundary conditions. Since the inverse heat transfer problems for the battery thermal model are ill posed where most parameters are unknown, the current study first focuses to make them clear, and section 2 illustrates the process of defining the unknown parameters and finally determining the ECs.

2.1. Battery Thermal Model. The lithium nickel manganese cobalt oxide ($LiNiCoAlO_2$: NCA) cylindrical-type battery cell is used in the current study. It is a typical battery of the so-called 21700 batteries with a size of 21.1 mm diameter and 70.15mm height. The nominal capacity is 4.9 Ah, and the charge/discharge voltage limits are 4.2 V and 2.5V, respectively. The specific technical specifications of the battery with are listed in Table 1.

To predict the battery thermal responses, it needs to realize how much heat is generated and dissipated during its operation, and the related energy equation [26] can be expressed in the following:

$$\mathrm{mc}_p \frac{dT}{\mathrm{dt}} = \dot{Q}_{\mathrm{gen}} - \dot{Q}_{\mathrm{dis}}, \tag{1}$$

where m, c_p, and dT/dt on the left-hand side are the mass, specific heat, and temperature changes (dT) over time (dt) of the battery cell. In the thermal analysis, the mass of the battery is 69.5 g, and the specific heat is defined by Equation (2), considering the temperature-dependent property of the LiBs.

$$c_p = 2.29 \bullet T_{\mathrm{cell}} + 1040.5. \tag{2}$$

Equation (2) is from the previous work by Sheng et al. [25], which analyzes the same type 21700 LiB as the current study. The first and second terms on the right-hand side of Equation (1) are the heat generation and heat dissipation of the battery, respectively. Since both the heat generation and heat dissipation are one of the major terms changing the battery temperature, more explanation for the battery heat generation is discussed more closely in the next section 2.2 and for the heat dissipation in the section 2.3. Given that the LiB is a composite material composed of five structural layers, it has anisotropic properties [27] with two thermal conductivities in the radial and axial directions. This may occur a thermal gradient within the battery cell depending on the experimental environments. It is required to use discretization methods, such as a finite element or difference, to solve the temperature distribution with the cell. However, it is beyond the scope of the current work and is not covered at this time. Instead, it is noted that the current study adopts the lumped thermal capacitance method after checking its applicability with the small enough Biot number (Bi) in all heat transfer directions. The Biot number in the radial

Table 1: Specifications of the battery cell.

Item (unit)	Value
Model	INR21700-50G
Manufacturer	SAMSUNG SDI
Cathode/anode materials	$LiNiCoAlO_2$/graphite
Electrical properties	
Nominal capacity (Ah)	4.9
Nominal voltage (V)	3.63
Charging/discharging voltage ranges (V)	2.5~4.2
Maximum current (A)	14.7 (3 C-rate)
Cycle life (end at 80% of nominal capacity)	1,000
Physical and thermal properties	
Dimension* (mm)	21.1×70.15
Mass (g)	69.5
Specific heat ($J \cdot kg^{-1} \cdot K^{-1}$)	$f = (T_{cell})$ [25]
Thermal conductivity ($W \cdot m^{-1} \cdot K^{-1}$)	$k_r = 1.16$, $k_z = 23.6$ [25]

*Diameter × Height.

and axial directions under the experimental conditions is estimated as

$$\begin{cases} \mathrm{Bi}_r = \dfrac{hL_c}{k_r} = \dfrac{9.965 \bullet 0.004594}{(1.16)} \approx 0.039464 < 0.1, \\ \mathrm{Bi}_z = \dfrac{hL_c}{k_z} = \dfrac{9.965 \bullet 0.004594}{(23.6)} \approx 0.000194 < 0.1, \end{cases} \tag{3}$$

with the maximum heat transfer coefficient (h) calculated in the current study to verify the model validity under the most rigorous condition as possible. The characteristic length (L_c) is calculated as the volume and surface area ratio for the cylinder. Considering the anisotropic characteristics of the battery, the higher value of thermal conductivities in radial (k_r) and axial (k_z) directions is applied in the calculation. Similar to the case of specific heat capacity, the values of two thermal conductivities are referred from the previous work by Sheng et al. [25]. Conclusively, as the Biot number in both the radial and axial directions is calculated as less than 0.1 [26], which is the criteria to apply the lumped capacitance assumption; the current study assumes there is no severe thermal gradient within the battery cell. In applying the lumped parameter model, the convective heat transfer coefficient (h) is a changeable parameter different from the properties of the battery, so the lumped model can be sufficiently applied by adjusting ambient conditions to natural convection or semiadiabatic conditions. In addition, in the base discharging experiment to obtain the data used for the developed model, as the experiments are intended to perform at low C-rate ranges (≤1.0C) where reversible heat is relative clear, the thermal gradient within the cell could be small with the uniform and low current density within the cell. The more descriptions on the experimental procedures are explained in the Chapter 3 (Experiment).

2.2. Battery Heat Generation. It has been known that there are four heat sources of irreversible resistive heat, reversible entropic heat, and heat in side reactions and mixing process involved in the battery heat generation. The first two heat sources are mainly involved in the battery thermal behavior as they are immediately responded to the internal resistance and entropy change of the battery during charge or discharge, so they are considered to be the most important in battery thermal analysis from almost all previous literature. The other two heat sources, the heat in side reactions and in the mixing process, are related to the aging process of the battery and due to the formation and relaxation of concentration gradients within the cell, which is significant in the dynamic charge or discharge cycle [28]. In addition, compared to the former joule and entropic heat, the latter two heat sources are recognized to be limited and can be negligible in general trend for electrochemical systems with good transport properties and for high-power applications [29]. Considering that the batteries used in the current study are new and tested under the constant C-rate, the irreversible resistive and reversible entropic heat are principally focused on. To sum up, the battery heat generation can be expressed as

$$\dot{Q}_{\mathrm{gen}} = I(U_{oc} - V_{\mathrm{cell}}) - \mathrm{IT}\frac{dU_{oc}}{dT}. \tag{4}$$

The former is the irreversible resistive heat due to the electrical loss by the internal resistance of the battery. It is proportional to the current I where the its sign is positive for discharge and negative for charge reflecting the open-circuit voltage (OCV, U_{oc}) is generally higher than cell voltage (V_{cell}) for the discharge case and vice versa for the charge case. Therefore, the resistive heat is always exothermic regardless of the sign of the current. The OCV is the electrical potential difference between the cathode and anode materials of the battery when there is no external load. Taking into account that the OCVs are critically varied by the state of charge (SOC) of the battery [24], it is necessary to characterize the OCV-SOC relation. Accordingly, the preliminary experiment is carried out to measure them for each state of charge, considering both the resistive ohmic and capacitive nonohmic sources by activation and mass concentration. The more precise description of the above experiment is written in section 3.2 of the experimental procedure. On the one hand, the latter is the reversible entropic heat by the entropy change (ΔS) between the cathode and anode materials of the battery. In contrast to the resistive heat, the entropic heat is either exothermic or endothermic depending on the signs of the current and entropic coefficient ($dU_{oc}/dT = \Delta S/nF$, EC), in which it is highly related to the electrochemical reactions occurring in LiBs and defined as the entropy change divided by the number of electron (n) and the Faraday Constant (F). The entropic coefficient in the current study is recognized as the thermal property related to the total microscopic change in entropy of within full cell of $LiNiCoAlO_2$ cathode and graphite anode since the entropy change in battery occurs between two active materials due to lithium

concentration change. The ECs are known to be greatly varied according to the state of charge of the battery, and The T in Equation (4) is the absolute temperature of the battery in degrees Kelvin.

2.3. Estimation of Heat Dissipation and Heat Transfer Coefficient. During operation, the battery not only generates the heat but also dissipates the heat. This battery heat dissipation is a heat loss to the surrounding environment during the experiment and generally consists of heat convection and heat radiation to the surroundings. Each heat transfer rate is different according to the shape of the battery or the experimental heat transfer conditions. In particular, the convective heat transfer coefficient is commonly estimated using empirical equations, such as the Nusselt number correlations. However, it is impractical to use the empirical correlation that entirely reflects the experimental conditions, and besides, the circulating airflow to keep the stable temperature inside the chamber could prevent to find the exact heat transfer coefficient. Therefore, the current study considers using another method to calculate the overall and optimal heat transfer coefficient that includes both the convective and radiative heat transfer coefficients. The adopted method is to track the temperature changes of the battery by cooling the battery for a certain period, estimating the cooling rates of the battery cell with the numerical algorithm. After finishing the discharge process, the battery heat generation is stopped as well, but the battery heat dissipation occurs continuously in nature, as seen in Figure 1(a). During the rest time, the battery is cooled down to the ambient temperature in the form of a nonlinear curve, and the energy equation for the battery during the rest time can be written in

$$\left(\mathrm{mc}_p \frac{dT}{dt}\right)_{\mathrm{cell}} = -\dot{Q}_{\mathrm{dis}}, \tag{5}$$

where the equation states that the increase or decrease rate of the internal energy of the battery cell is varied by the heat dissipation rate ($\dot{Q}_{\mathrm{dis}}$). When considering Newton's law of cooling, the heat dissipation rates can be calculated by

$$\dot{Q}_{\mathrm{dis}} = hA(T_{\mathrm{cell}} - T_{\mathrm{amb}}), \tag{6}$$

where h, A, and $(T_{\mathrm{cell}} - T_{\mathrm{amb}})$ denotes the heat transfer coefficient, heat transfer surface area, and temperature difference between the cell and the ambient. Here, the optimal value of the heat transfer coefficient can be obtained by solving the nonlinear cooling curves of the battery cell obtained during the rest time displayed as the blue line in Figure 1(a). In the present work, the nonlinear problems are solved based on the generalized reduced gradient (GRG) algorithm. The GRG algorithm is the typical gradient-based numerical method often used for constrained and nonlinear optimization problems [30]. It is similar to the widely known gradient descent algorithm [31], which is an iterative first-order optimization algorithm used to find the optimal value that minimizes the cost function, as seen in Figure 1(b). The cost function is directly the error here, and by reducing the errors, it is possible to find the optimal heat transfer coefficient for each experimental case. The related equation form is expressed as

$$h = \mathrm{argmin}\left[\left(mc_p \frac{dT}{dt}\right)_{\mathrm{cell}} - hA(T_{\mathrm{amb}} - T_{\mathrm{cell}})\right]. \tag{7}$$

The term in the square bracket of Equation (7) are the Equation (6) and states that the change rate of the battery thermal state (left term in square bracket) is equal to the cooling heat transfer rate from the cell to ambient (right term in square bracket). To sum up, Equation (7) means that the optimal h value can be found in the direction in which the sum of those two terms is minimized since the summation should be theoretically zero. In this study, the error is defined as the mean square error (MSE), which is the square of the difference between the two terms. For the iterative computations, the initial guess for h is set to $1\,\mathrm{W{\cdot}m^{-2}{\cdot}K^{-1}}$, and Figure 1(b) describes the process of finding the optimal value that minimizes the gradient, i.e., MSE through iterative computations. For instance, the battery temperature curves according to h values obtained from the iterative calculations are depicted in Figure 1(c). It also can be seen that the finally computed optimal h predicts the battery temperature most similar to the actual experimental value. The convergence criteria to stop the iteration is set to be 10^{-6}. The GRG algorithm is solved using Microsoft® Excel's Solver® add-in tool [32], which is a powerful solver based on a spreadsheet to optimize the nonlinear least squares data fitting. In practice, the cooling period used in the numerical iterations is the first 1 h during which reveals a clear temperature change, as shown in Figures 1(b) and 1(c). The heat transfer coefficients for experimental cases are computed as values ranging from $8.127\,\mathrm{W{\cdot}m^{-2}{\cdot}K^{-1}}$ to $9.965\,\mathrm{W{\cdot}m^{-2}{\cdot}K^{-1}}$, and then used for the proposed method to determine the ECs that is explained more clearly in the next section 2.4. The accuracy of the GRG algorithm to find the optimal h is verified together during the validation process in section 4 (results and discussion).

2.4. Calculation of Entropic Coefficient Using Inverse Heat Transfer Analysis. All parameters except the ECs needed for the battery thermal model are determined from the above subsections 2.1 to 2.5. Therefore, it can be seen that the EC is the only unknown parameter in the energy equation (Equation (1)) of the battery cell, and the prerequisites for solving the inverse heat transfer problem are established. If viewed as inverse heat transfer problems, the ECs can be inversely rearranged by

$$\frac{dU_{oc}}{dT}(t) = \frac{mc_p(dT/dt) - I(U_{oc} - V_{\mathrm{cell}}) + hA(T_{\mathrm{cell}} - T_{\mathrm{amb}})}{\mathrm{IT}_{\mathrm{cell}}}. \tag{8}$$

The above proposed process is named as the inverse heat transfer analysis (IHTA) method for a clear description. It is noted that the ECs are calculated transiently, considering the battery heat generation is not constant. In solving the above

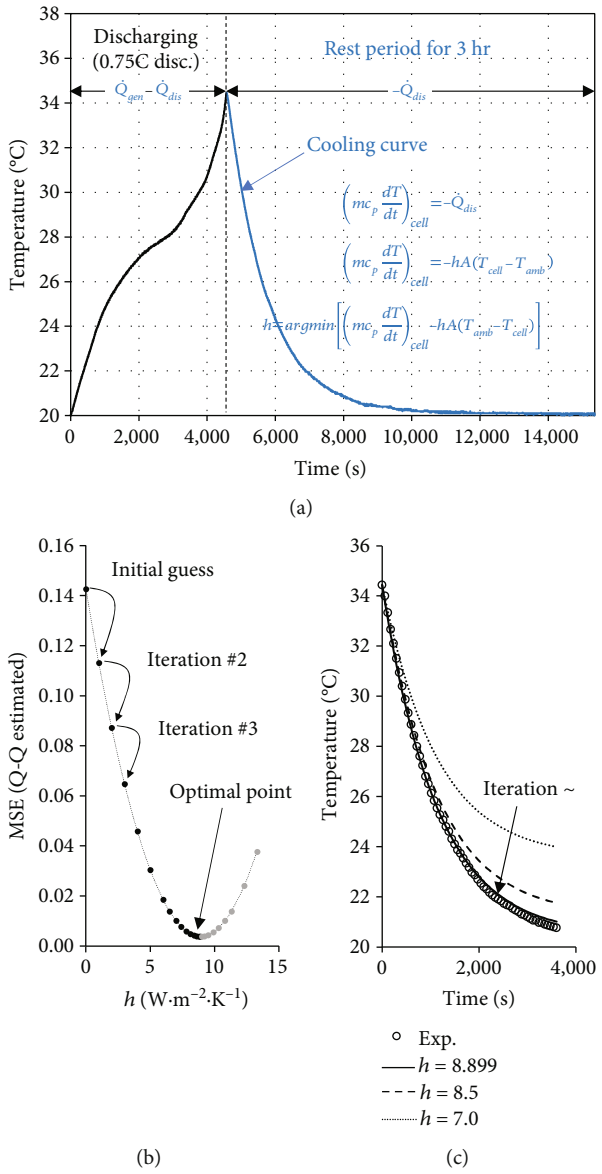

FIGURE 1: (a) Temperature changes of the battery during discharging (black line) and 3 hours rest period (blue line), (b) iterative process to find the optimal heat transfer coefficient by minimizing the error, and (c) resulted battery temperatures during 1 hour cooling period.

equation, the time step (dt) is required to be set as appropriate to secure sufficient temperature changes of the battery (dT) as it is one of the key variables in the IHTA method. Since the battery temperature will change according to its heat generation rates, it will not change enough if the dt is too short as 1 second for instance. Contrary, If dt is too long, the ECs cannot be obtained densely enough according to battery SOCs. From this point of view, the current study sets dt as a value by diving the total data by a hundred to calculate the EC every 1% SOC. Four discharge cases with different C-rates (0.25C, 0.5C, 0.75C, and 1.0C) are applied for the IHTA method to confirm whether the ECs vary according to the C-rate and to secure sufficient ECs according to SOC at the same time. The cell voltage and temperature curves used to build the IHTA method are shown Figure 2.

Since the total discharge time of the battery is different for each C-rate condition, it is necessary to organize the derived ECs under the same criteria rather than time (t). Thus, the time-dependent ECs are converted to as a function of SOC as

$$\frac{dU_{oc}}{dT}(t) \longrightarrow \frac{dU_{oc}}{dT}(\mathrm{SOC}). \tag{9}$$

The SOC of the battery is estimated using the coulomb counting method considering operational efficiency [33], and its equation form is expressed in

$$\mathrm{SOC}(t) = \mathrm{SOC}(t-1) - \int \frac{I}{3{,}600 \bullet C_{\mathrm{rated}} \bullet \eta}\,\mathrm{dt}, \tag{10}$$

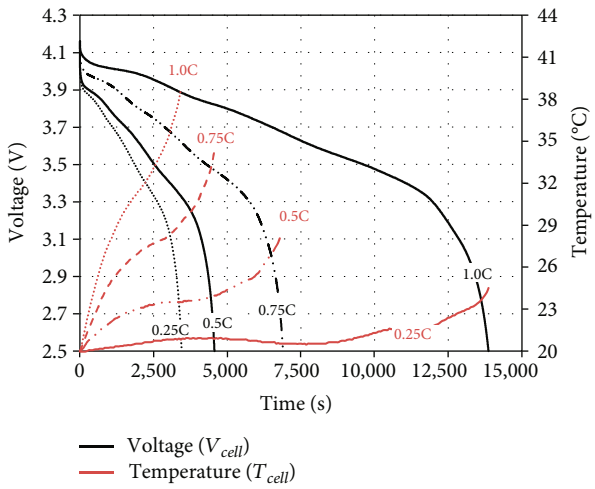

FIGURE 2: Voltage and temperature curves during four discharging processes.

where the C_{rated} is the 4.9 Ah rated capacity of the battery. For all experimental cases, the initial SOC of the battery is fully charged by 100% for equal analysis. A more related experimental method is described in chapter 3. The operational efficiency (η) is calculated by the ratio of discharged or charged capacity per rated capacity, as shown in the following:

$$\eta = \frac{\sum_{i=1} I_i t_i}{C_{\text{rated}}} = \frac{I_1 t_1 + I_2 t_2 \cdots}{C_{\text{rated}}}, \tag{11}$$

where the I_i and t_i are the charging and discharging currents and time periods, respectively. For the final task, the regression analysis on calculated ECs is to obtain the representative EC values. The regressed ECs are then optimized though the least squares estimation to reduce the error deviation between the measured value (y_i) and calculated value ($\hat{y}_i$) as expressed in

$$\frac{dU_{oc}}{dT}(\text{SOC}) = \text{argmin} \sum_{i=1}^{n} (y_i - \hat{y}_i)^2. \tag{12}$$

In this study, the five regression models, a polynomial, rational, sum of sine, Fourier's series, and smoothing cubic splines, are adopted for the regression analysis. Each model is then optimized via least squares estimation in the direction in which the difference, $(y_i - \hat{y}_i)^2$, between the measured and calculated value decreases. The related information about each regression model and the selection process of the best regression model are detailed in section 4.1 (determination of entropic coefficients).

2.5. Potentiometric Method. In order to confirm the feasibility of the ECs obtained from the developed IHTA method, it is needed to compare them with those calculated from the existing potentiometric (PM) method. In the PM method, the ECs are determined by the voltage change in relation to the temperature change. Therefore, the PM method in the current study is conducted by measuring the OCVs at five different temperatures of 15°C, 25°C, 35°C, 45°C, and 55°C, as shown in Figure 3(a), which shows the experimental protocols of tracking the voltage changes at 100% SOC, for instance, according to the temperature changes. At each temperature range, the battery is rested enough for a while to reach the electrical equilibrium state, and the rest time is set as 3 h by confirming the voltage is changed. Hence, it takes 18 h experimental time per one SOC point. From the measured voltages, the ECs are determined by calculating the slope of the voltages to the temperatures, as depicted in Figure 3(b), and it is realized that the EC at 100% SOC is positive as the voltage is in the linear relation with the temperature. The same measurements are repeated from 100% to 0% SOC at 10% SOC intervals to calculate the ECs at other SOC ranges. The ECs intermittently measured by the PM method are then compared with those by the IHTA method, and the comparison results are described and discussed in section 4.2.

3. Experiment

3.1. Experimental Setup. The photos of the experimental equipment are depicted in Figure 4(a). In the battery experiment, a battery cycler (PEMC 50-60, PNE Solution Co., Ltd., Republic of Korea) is used to load the battery cell, and the set multimeter (34401A, Keysight Technology, Inc., United States) measures the applying current and cell voltage in real-time. The multimeter with built-in ampere meter measures the direct current flowing via the electrical cables and likewise built voltage meter measures the cell voltage with voltage sensors, which are directly connected to the battery jig as shown in Figure 4(b). The battery cell is fixed with a battery jig and installed inside the environmental test chamber (THC576, JinSung-PLT Co., Ltd., Republic of Korea), which controls the air conditions. Both the battery cycler and environmental test chamber are connected to the Control PC, which gives the commands to both equipment together. The lateral surface area of the battery is covered with the 10 mm thickness insulator to protect from the unexpected fluctuation of airflow inside the chamber, which might cool the battery unevenly. A total of six T-type thermocouples (TT-T-3-K, Junkyoung Instrument & Electric, Republic of Korea) is used to measure the temperature: four for battery temperature (the blue colored sensors is the safety sensor for emergency), and two for ambient air and surrounding wall temperatures, respectively.

The 21700 battery cell used in the experiment and the temperature measurement points for the battery is shown in Figure 4(c). To observe the surrounding environment around the battery cell, the temperature of the air space next to the battery and the wall of the chamber is measured together. All temperature data are accumulated to the data acquisition system (PX1000, Yokogawa Electric Co., Ltd., Japan). The data acquisition system is connected to the control PC to acquire the data of the applying current and cell voltage at the same time. The main specifications of experimental equipment with measurement accuracies are summarized in Table 2. The experimental schematic is

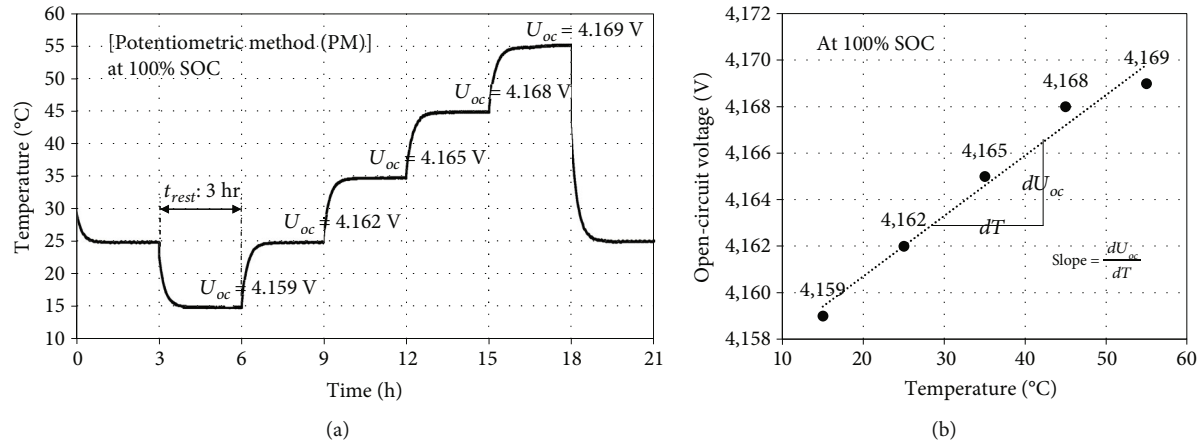

FIGURE 3: (a) Experimental protocol of potentiometric method, and (b) the calculated entropic coefficient at 100% state of charge.

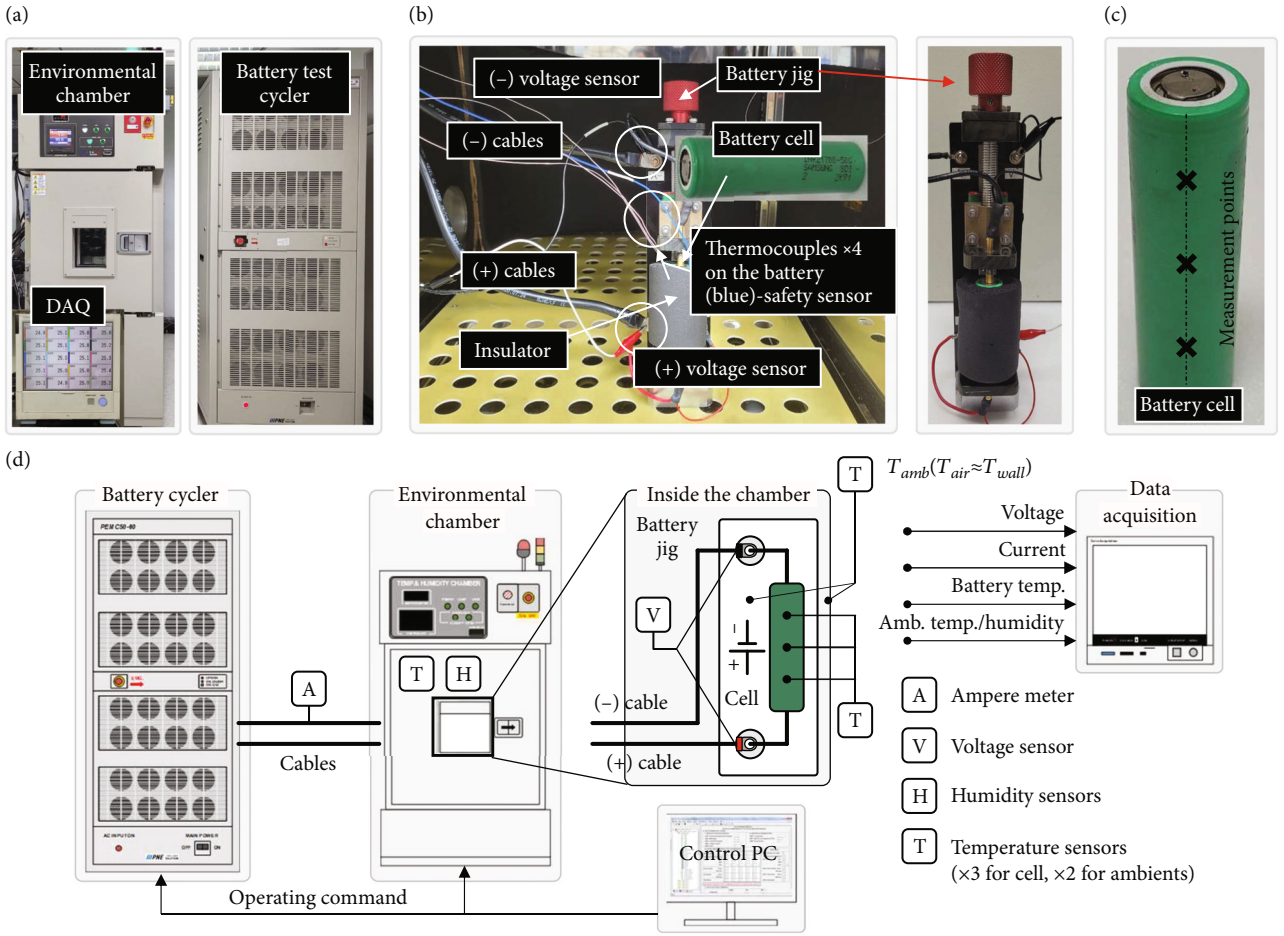

FIGURE 4: (a) Photos of main experimental equipment, (b) inner view of environmental chamber, (c) battery cell and temperature measurement points of battery cell, and (d) installation diagram.

illustrated in Figure 4(d), which shows the overall installation diagram of the battery experiment and the process of the data measurement and acquisition processes.

3.2. Experimental Procedure. The battery experiment is largely divided into two processes of discharging and charging. Both are basically operated on constant current (CC) mode, but in the case of charging, the battery is charged with the constant current-constant voltage (CC-CV), which the battery is initially charged with the CC mode, and converted to the constant voltage (CV) mode when the battery voltage reaches the upper limit voltage of

Table 2: Specifications of experimental equipment and measurement accuracy [34].

Equipment	Manufacturer	Model	Operating range	Accuracy (F. S)
Battery cycler	PNE solution	PEMC 50-60	0 ~ 50 V	±0.1%
			0 ~ 120 A	±0.1%
Environmental chamber	JinSung PLT	THC576	-20~80°C	±0.5 °C
Thermocouple	JIS-28G-TEF-T	T-type	-50~200°C	±0.5 °C

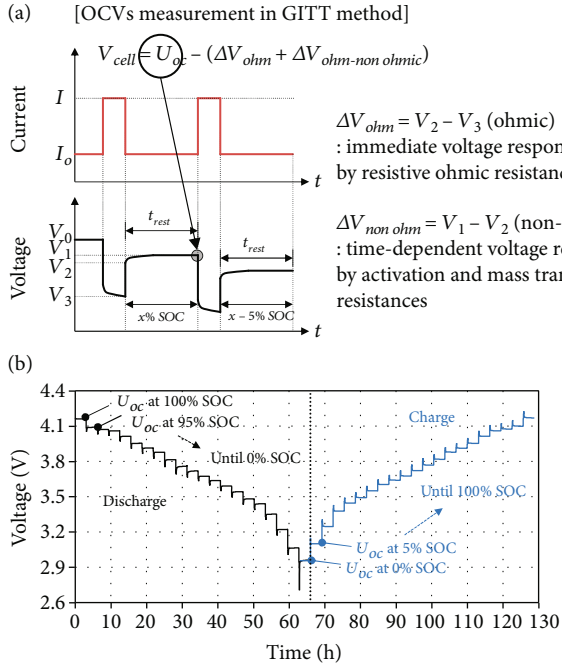

Figure 5: (a) Current and voltage profiles in the GITT, and (b) open-circuit voltages measurement during discharge and charge cycle.

Table 3: Open-circuit voltages per state of charge [34].

SOC (%)	Discharge	Charge
100	4.162	4.173
95	4.091	4.102
90	4.072	4.077
85	4.061	4.062
80	4.014	4.015
75	3.954	3.955
70	3.914	3.913
65	3.878	3.88
60	3.814	3.819
55	3.767	3.767
50	3.718	3.722
45	3.673	3.677
40	3.636	3.641
35	3.590	3.605
30	3.540	3.551
25	3.480	3.494
20	3.438	3.447
15	3.349	3.378
10	3.219	3.246
5	3.061	3.101
0	2.957	2.957

4.2 V to prevent overcharging. At the CV mode, the charging voltage remains constant at 4.2 V, and the charging current is reduced gradually until reaching the predefined current, which is set to be 123 mA in the current study. All the set voltage and current values are referenced from nominal specifications in the specification of product provided by the manufacturer [35]. Prior to the main experiments, the preexperiment of galvanostatic intermittent titration technique (GITT) is adopted to preferentially measure the OCVs of the battery at certain SOC levels. It subjects the cell to intermittent current pulses alternating between a CC charge or discharge and a relatively long rest time [36], and its measurement process is illustrated in Figure 5. Figure 5(a) shows the case of discharging process where the battery voltage drops immediately in response to the applied current. When the applied current is stopped, the immediate (ΔV_{ohm}) and time-dependent (ΔV_{nonohm}) voltage responses during the rest time are detected. As they are widely known as related to the resistive ohmic and capacitive nonohmic sources by activation and mass concentration in the electrochemical system, the OCVs in the GITT are considered both the ohmic and nonohmic resistances. Specifically, the applying C-rate in the GITT is set to 0.2C (980 mA) of standard C-rate of the battery [35], and the rest time is set as constant 3 h after checking that the time is sufficient enough for the battery to reach the electrical-thermal equilibrium state [37]. To protect the battery from the undesired degradation on cell's lifetime and performance, the initial environmental conditions for the battery are kept at normal temperature (20°C) and pressure (1 atm) conditions [38].

As shown in Figure 5(b), the OCV measurements are first measured during the discharge process by intermittently discharging the battery by 5% SOC interval from 100% SOC to 0% of the fully discharged state, and then vice versa intermittently charged the battery with the same operating conditions as discharging conditions to likewise measure the OCVs at the charge process. The data of open-circuit voltages per state of charge measured by the above GITT method are presented in Table 3. The entire experimental procedures are comprised as follows and

Table 4: Experimental procedures for model development and analysis.

No.	Mode*	C-rate (C)	T_{amb} (°C)	Objective or remark
1	Disc.	0.25, 0.5, 0.75, 1.0		Derive entropic coefficients
2	Disc.	0.25~2.0		Method validation
3	Char.	0.50	20	Analysis on charging effects
4	Disc+char.	Dynamic		Analysis on variable state of charge
5	Driving cycle	Dynamic		US06 drive cycle (dynamic load)
6	Disc.	0.50	10, 20, 30	Analysis temperature effects

*Disc: discharge; Char: charge.

Table 5: Uncertainty analysis of measured and calculated parameters [34].

Parameter (symbol or equation)	Unit	Typical value	Uncertainty
Ambient temperature (T_{amb})	(C)	20	±0.5
Battery temperatures (T_{cell})	(C)	20	±0.2887
Open-circuit voltage (U_{oc})	(V)	4.162	±0.0004162
Cell voltage (V_{cell})	(V)	4.2	±0.00042
Current (I)	(A)	32	±0.032
State of charge (SOC)	(%)	99.03	±0.000009662
Resistive heat ($I(U_{oc} - V_{cell})$	(W)	3.901	±0.05494
Heat dissipation ($\dot{Q}_{dis}$)	(W)	1.632	±0.03302
Entropic coefficient (dU_{oc}/dt)	(mV·K^{-1})	0.6395	±0.02224

tabulated in Table 4. To begin with, the four base experimental cases discharging from 0.25C to 1.0C at intervals of 0.25C (No.1) are performed for applying the developed IHTA to derive the ECs according to the SOC. In order to obtain continuous temperature data in the entire 0 to 100 SOC ranges, the battery is preferentially charged to the 100% SOC first, and then fully discharged fully discharged to 0% SOC with the predefined C-rate. Afterward, the other discharging cases are used for model validation under different C-rates of low to high C-rate conditions (No. 2). The validation objective of experiment No. 2 is to find out whether the finally derived ECs are applicable in any C-rate cases. The remaining is for the verification and in-depth investigation of the developed method under various operating conditions. The first one is the validation under charging process (No. 3) to check its feasibility under different charging rates based on the background that EC is highly dependent on the battery SOC. The second one is the validation under dynamic load conditions (No.4 and 5), of 10°C to 30°C. The dynamic load conditions are divided into two modes; one is the artificially made cycle composed of repetitive discharging and charging process for a certain period with different but constant C-rates, and the other is the dynamic load conditions with very irregular current profiles after the US06 drive cycle. The last case is the validation under different ambient temperatures (No. 6). It is likewise to confirm the effective temperature ranges that the ECs are valid to accurately calculate the battery heat generation. The objectives or remarks of each experimental procedure are listed in Table 4 together.

3.3. Uncertainty Analysis. The uncertainty on the parameters used in this study is analyzed to ascertain their accuracies, and the results of the uncertainty analysis are summarized in Table 5. The uncertainty of the parameter is generally obtained as the sum of the systematic and random errors in the steady state experiment. The former one is the instrumental or fixed error, which is related to the measurement accuracy of the instruments, and is often provided as a constant of percentages error as shown in the rightmost column of Table 2. The latter one is the unpredictable changes in the experiment. It is usually estimated by the standard deviation of the measured data in the steady-state experiment but not considered in the transient experiment, where the measured parameters vary in real time [34]. In this regard, the uncertainty is mainly estimated with the instrumental errors for the measured parameters. The uncertainty of the calculated parameters is calculated by the error propagation using the root-sum-square method as expressed in

$$\delta R = \left\{ \sum_{i=1}^{n} \left(\frac{\partial R}{\partial X_i} \delta x_i \right)^2 \right\}^{0.5} = \left\{ \left(\frac{\partial R}{\partial x_1} \delta x_1 \right)^2 + \left(\frac{\partial R}{\partial x_2} \delta x_2 \right)^2 + \cdots + \left(\frac{\partial R}{\partial x_n} \delta x_n \right)^2 \right\}^{1/2}, \quad (13)$$

where the ∂R, and δx_i are the overall uncertainty of the calculated parameter and the uncertainty of each individual

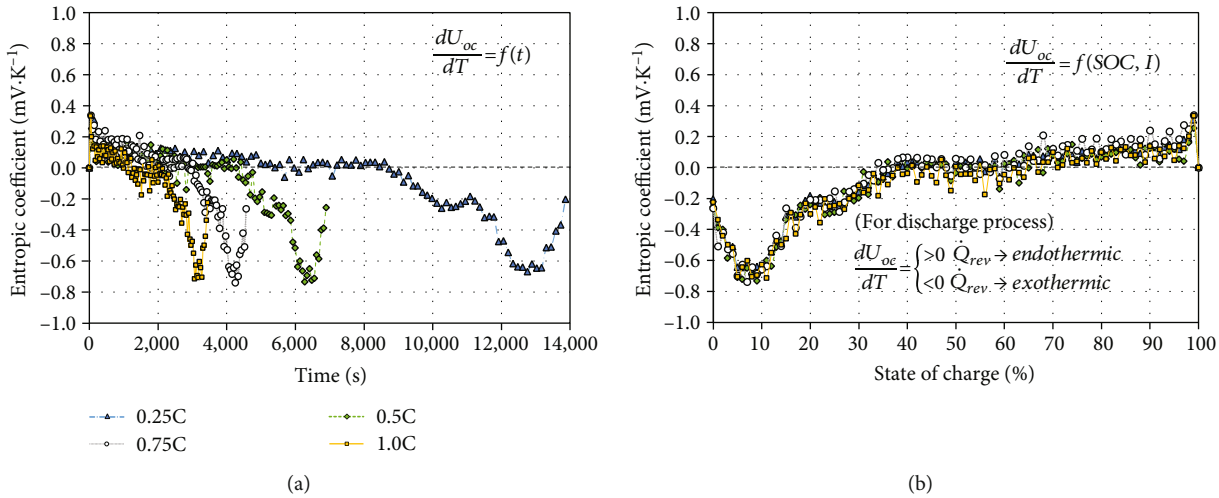

Figure 6: Determination of entropic coefficients according to (a) time and (b) state of charge of the battery using inverse heat transfer analysis method [39].

measured parameter, which is used to estimate the calculated parameter. The results are presented in Table 5 with the typical values and maximum uncertainties from the uncertainty analysis. Hence, the remaining uncertainties of other values of each parameter are lower than the listed values. Accordingly, it is realized that the experimental data is reliable for further investigation.

4. Results and Discussion

4.1. Determination of Entropic Coefficients. From the experimental results of battery experiments, the four cases of discharging at 0.25C, 0.5C, 0.75C, and 1.0C are utilized for determining new ECs according to the SOC of the battery. Following the step-by-step process of the IHTA method, the new ECs are derived as the continuous form of the time function as shown in Figure 6(a). The total discharge time of the battery is inversely proportional to the applying C-rate when fully discharged from the fully charged state, so the case of lowest, 0.25 C, recorded the longest discharge time, and conversely, the case of highest, 1.0 C, recorded the shortest discharge time. It is remarkable that the calculated ECs of all cases show a very similar trend, decreasing with time and then increasing rapidly before ending. To compare the trends of each case under the same standard, the ECs are rearranged as a function of SOC as shown in Figure 6(b), and it is confirmed that the trends of calculated ECs are almost the same in line with the battery SOCs despite discharging at different C-rates.

From the results, the values of EC to depend highly on SOC are confirmed, as known in the previous literature, and the applicability of the IHTA method is demonstrated. In the view of SOC, the ECs are positive in the 60-100% range and remain nearly zero in the middle state of 40-60%, and negative at SOC less than 40%. Reminding the reversible entropic term in Equation (8), it can be seen that the entropic heat is endothermic for negative EC, and in the opposite, it is exothermic for positive EC when the battery is discharged. However, as mentioned above, the sign of reversible heat changes by the sign of the current (positive for discharge and negative for charge) as well as the EC. In this respect, the former endothermic reaction becomes the exothermic reaction and vice versa during the charging processes. To obtain the representative ECs applicable to all operating conditions, regression analysis is attempted for the derived data. The EC data in Figure 6(b) has the anomalous feature consisting of multiple local inflection points depending on the battery SOC, requiring the high-order equations for the regression analysis. Moreover, since the data can be positive or negative depending on the battery SOC, the regressed equation should reflect it. In this regard, the five regression models, polynomial, rational, sum of sine, Fourier's series, smoothing cubic splines, are adopted for the regression analysis considering their equations form. Through the least squares estimation following Equation (12), the five regression models are optimized to well predict the ECs according to battery SOC. The least squares estimations are conducted with the MathWorks® Matlab curve fitting toolbox™ [40]. The results of the least squares estimation are depicted in Figure 7 with the profiles of optimized regressed models with the total.

The results from regression models of polynomial, rational, sum of sine, Fourier's series are illustrated in Figure 7(a), and the remaining smoothing cubic spline is shown in Figure 7(b), respectively. It is noticeable that all methods predict well the tendency of the EC according to the SOC, and for further investigation, the most precise method is selected for further investigation. The accuracy of each model is listed in Table 6 in terms of sum square error (SSE), R-square (R^2), and root mean square error (RMSE), and the methods of each model and equation forms specifically for the regression models are listed together. Among the various models, the most accurate model is determined based on the criteria of R^2, and the smooth spline model in Figure 7(b) is finally chosen for the subsequent analysis. Compared to the other four models,

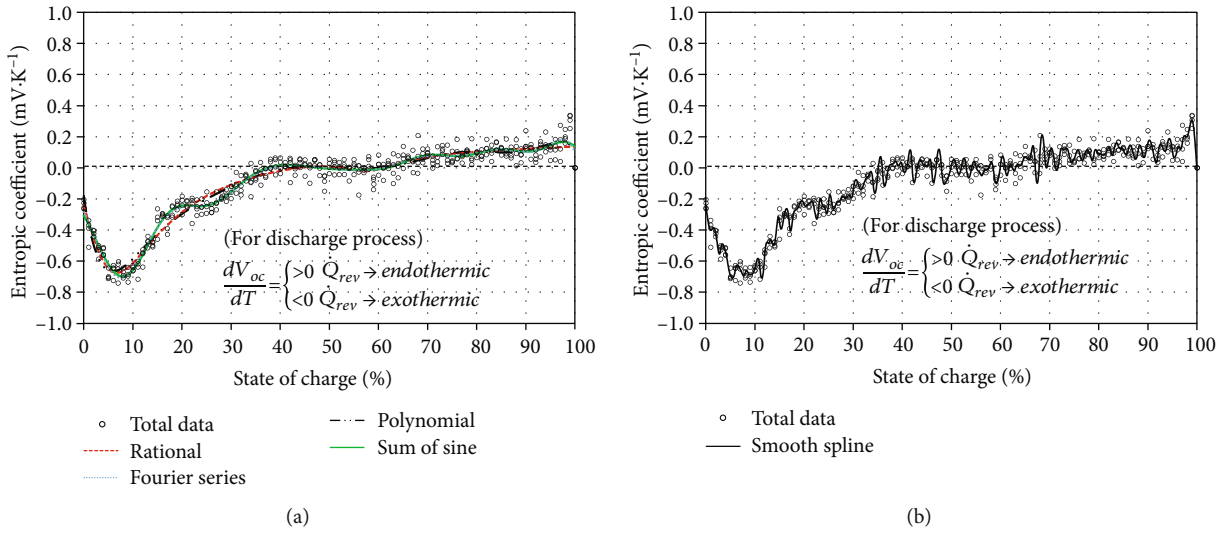

Figure 7: Profiles of the entropic coefficients according to various regression models: (a) polynomial, rational, sum of sine, Fourier's series, and (b) smooth spline.

Table 6: Results of regression with least-squares estimations.

Model	Method	Equation	Order	SSE	R^2	RMSE
Smoothing spline	Cubic spline least squares	—	—	0.615	0.973	0.0454
Polynomial	Linear least squares	$\sum_{i=1}^{n+1} a_i x^{n+1-i}$	9	1.401	0.939	0.0596
Rational	Nonlinear least squares	$\sum_{i=1}^{n+1} b_i x^{n+1-i} / \left(x^m + \sum_{i=1}^{m} a_i x^{m-i} \right)$	4/4*	1.384	0.940	0.0592
Sum of sine	Nonlinear least squares	$\sum_{i=1}^{n} a_i \sin(b_i x + c_i)$	8	1.108	0.952	0.0540
Fourier series	Nonlinear least squares	$a_0 + \sum_{i=1}^{n} a_i \cos(iwx) + b_i \sin(iwx)$	7	1.084	0.953	0.0529

*Degree of denominator/numerator.

the smooth spline is considered to best reflect the tendencies of ECs, which are highly and randomly distributed according to the battery SOC.

A similar trend in ECs according to the SOC of the above result is very noteworthy. Entropy heat is literally the heat generated due to the entropy change within the internal structure of the battery [41]. That is, the state of the battery changes due to the transport of lithium ions and electrons whenever charging or discharging occurs. In other words, when fully charged, they are extremely concentrated toward the positive side when discharged to the negative side. At this time, the battery is in a very unstable state. Ideally, it can be seen that the battery is in the most stable state when the entropy coefficient is 40-60% SOC, which is close to zero.

4.2. Comparison with Existing Method. The ECs in the PM method are calculated by the slopes of voltage changes in relation to temperature changes and indicated in Figure 8 with those calculated from the IHTA method. Three calculated ECs by the PM methods are displayed with the ECs

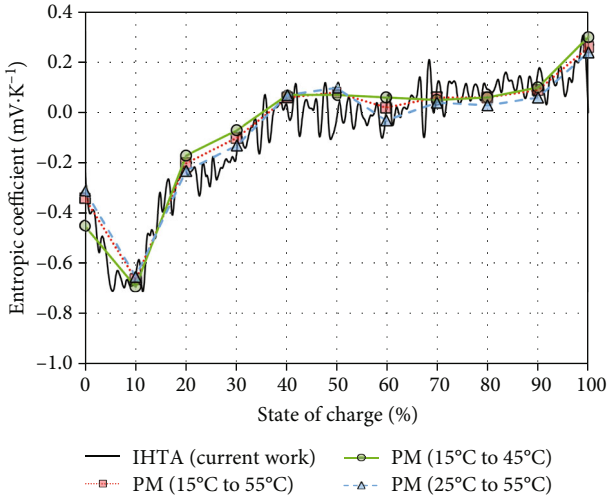

Figure 8: Entropic coefficients calculated from potentiometric and proposed methods.

Table 7: Comparison of conventional and proposed method to estimate the entropic coefficients according to state of charge.

	Potentiometric method	Proposed IHTA method
Equation	$(dU_{oc}/dT)(\mathrm{SOC})$	$(dU_{oc}/dT)(\mathrm{SOC}) = mc_p(dT/\mathrm{dt}) - I(U_{oc} - V_{\mathrm{cell}}) + hA(T_{\mathrm{cell}} - T_{\mathrm{amb}})/IT$
Method	Experiment	Experiment + numerical + analytical
Equipment	Environmental chamber + battery cycler	Environmental chamber (optional) + battery cycler
Measurement	Intermittent (5 temp. points & 11 SOC points)	Continuous (entire SOC ranges)
Time*	Total 198 hours (18 h per SOC)	12 hours 20 min (+1 h rest time per each disc case)

*Pure experimental time to estimate the entropic coefficients in the current study.

from the IHTA method. Though the ECs change slightly depending on how many voltage-temperature ranges are used to calculate the slope, it is identified that the overall trends of the calculated ECs from the two methods are found to be consistent, proving the feasibility of the proposed IHTA method.

Both PM and IHTA methods basically rely on the experiment to determine the ECs. However, there is a difference that the former completely depends on the experiment, whereas the latter minimizes the experiment by utilizing the numerical and analytical methods together. The differences between the two methods are summarized in Table 7. To begin with the required equipment for the experiment, both methods use the battery cycler and the environmental chamber, but it is noted that the environmental chamber is not essential for the proposed method because it can calculate the heat dissipation rates using the data during the rest time. Nevertheless, it is recommended to use the chamber to reduce the experimental uncertainties as possible. In the view of measurement, the PM method measures the ECs per each SOC intermittently, so it inevitably depends on linear interpolation between the intermittent values to predict the ECs for the entire SOC ranges. On the other hand, the IHTA method can obtain continuous ECs according to the SOC, so it can flexibly and precisely predict the battery thermal responses at any SOC. Lastly, the PM method requires 18 h per each SOC-step to track the voltage changes according to temperatures by repeating the process of changing temperatures and taking a rest, as shown in Figure 8. Thus, it takes a total 198 h considering the same processes are repeated for 11 SOC points of 0 to 100% SOC with 10% interval. In contrast, the proposed IHTA method takes a total of 12 h and 20 min : 500 min for the four discharge experiments and 240 minutes for cooling the battery during the rest time. From this viewpoint, the IHTA method can reduce the experimental time by at least over 93.8% compared to the potentiometric method. The required times above are the pure experimental time required to estimate the ECs in the current study. From the literature review, it is noted that the rest period, SOC, and temperature ranges for the PM method may vary from battery to battery because the size, material, or electrochemical properties of LiBs are not equal. In general, It is common to find that the PM method takes several days to several weeks in previous literature [15, 42, 43]. From this point of view, the proposed method can save experimental time while ensuring accuracy in determining the ECs.

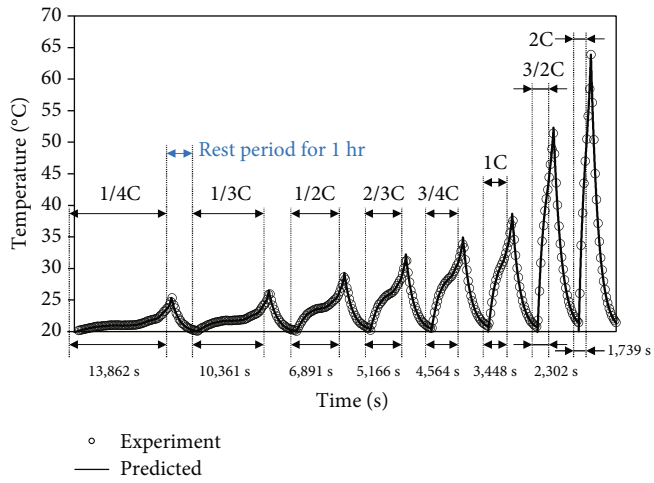

Figure 9: Validation of IHTA method under different current rates.

4.3. Method Validation and Discussion

4.3.1. Discharge Process with Different Current Rate. The representative ECs per battery SOCs estimated from the smooth spline regression model are used to calculate the reversible entropic heats of experimental cases. In addition to the four cases adopted for the model development, experimental cases of low (<1.0C) to high (>1.0C) C-rates ranging from 0.25C to 2.0C are used to verify the validity of the developed IHTA method. The validation is conducted in terms of the temperature changes of the battery during operation, and the experimental temperatures are directly compared with the simulated temperatures, which are predicted from the battery thermal model when using the above representative ECs obtained from the smooth spline regression model. The validation results are shown in Figure 9, where the temperatures measured from the experiment are depicted in circle symbols, and the predicted temperatures are displayed as the black line.

The experimental values are actually measured every second, but for the sake of clear visibility, they are expressed every 200 seconds. Not only for the period of battery operation (displayed with certain C-rate), but also for the rest period for 1 h is compared to validate the GRG algorithm used to obtain optimal heat transfer coefficients in section 2.3. With the maximum RMSE of 0.36°C, it is judged that both the IHTA method to calculate the ECs of the battery

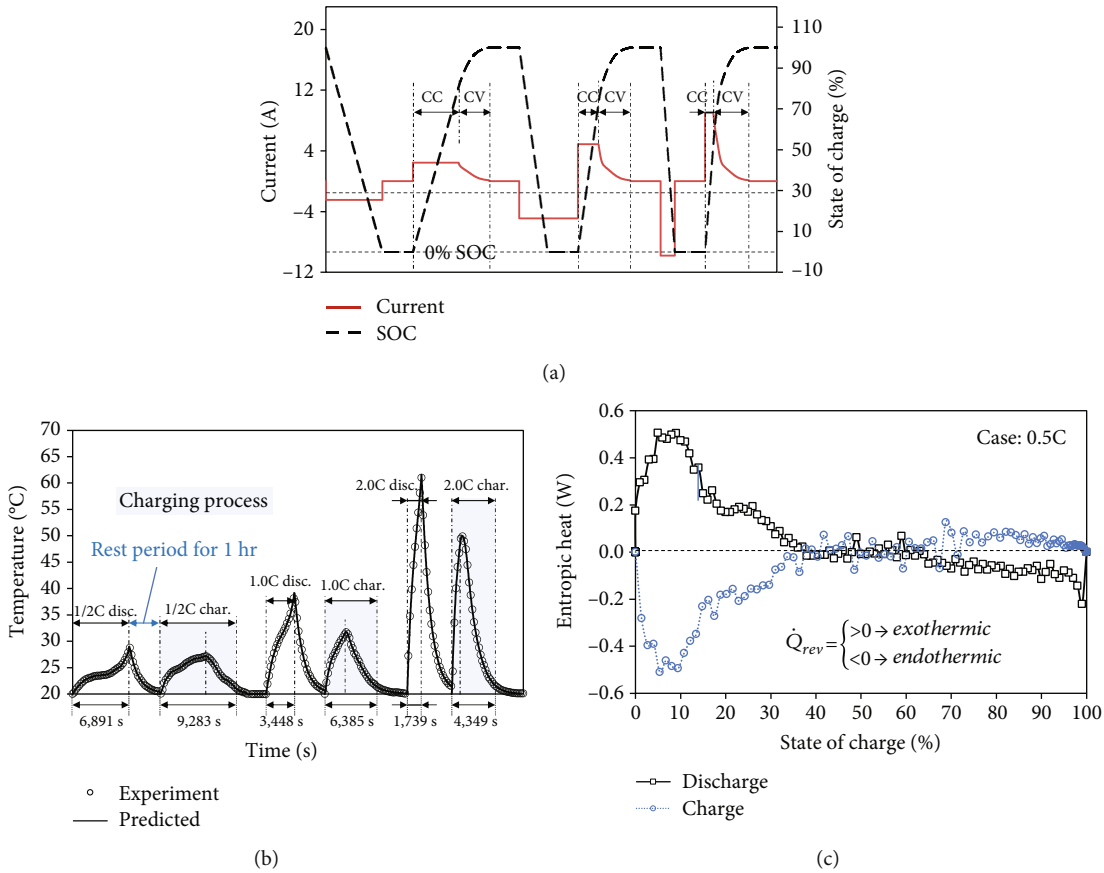

Figure 10: Comparison of discharging and charging process in the view of (a) current and state of charge, (b) battery temperatures, and (c) entropic heat for 0.5 C-rate.

per SOC and the GRG algorithm to find the optimal heat transfer coefficients are well validated and prove its applicability for further studies. From the above results, the battery temperature rises rapidly as the C-rates increases. Recalling the Bernardi equation in Equation (2), the resistive joule heat is proportional to the square of the current while the reversible entropic heat is proportional to the current. Therefore, it can be realized that the heat resistive heat contributes more to the battery heat generation than the reversible heat. This can be seen from the temperature curves that the curves become sharper as the C-rate increases.

4.3.2. Charge Process. In the previous section, the validation is carried out, focusing on the discharging process in which the battery SOC decreases linearly. Therefore, for the next proof of the proposed IHTA method, it is required to verify its applicability in the charging process conversely. Unlike the discharging process, the charging process is composed of two operating modes of CC and CV. Equal to the discharging process, the charging process is initially begun with the CC mode (0.5C in this case) and then converts to the CV mode when reaching the maximum cut-off voltage of 4.2 V to protect the overcharge of the battery. In the CV mode, the charging current is exponentially reduced until the predefined current, which is set to be 123 mA in the current study. The overall current profiles under 0.5C, 1.0C, and 2.0C processes are illustrated in Figure 10(a) with the resulting battery SOC. The current profile of the 0.5C, 1.0C, and 2.0C discharge cases is indicated together to clarify the difference among charging processes. The verification is conducted likewise in the view of the temperature variations of the battery as seen in Figure 10(b), and the calculated ECs are applicable in the charging process as well, revealing the maximum RMSE of 0.848°C. From the results, it is realized that the temperature profiles between charging and discharging processes are dissimilar even though the same C-rate is applied to the battery. In general, the temperature increases under all charging processes are overall low that it is due to the existence of CV mode where the applying current decreases gradually, in which means the total battery heat generations are likewise decreases. Besides, the unusual trend in the temperature profile is depicted in the case of low 0.5C discharging and charging cases. The temperature profile of the 0.5C discharging process appears the concave upward shape, where the uptrend of temperature increases quite linearly at the low SOC ranges (<40% SOC), becomes slow at the middle SOC ranges (40% ≤ SOC ≤ 60%), and again rapidly grows up at the high SOC ranges (>60% SOC). On the other hand, the opposite trend is realized in the case of charging, where the overall trend of the battery temperature draws the concave downward shape in respect to time. This is because the signs of the charging and

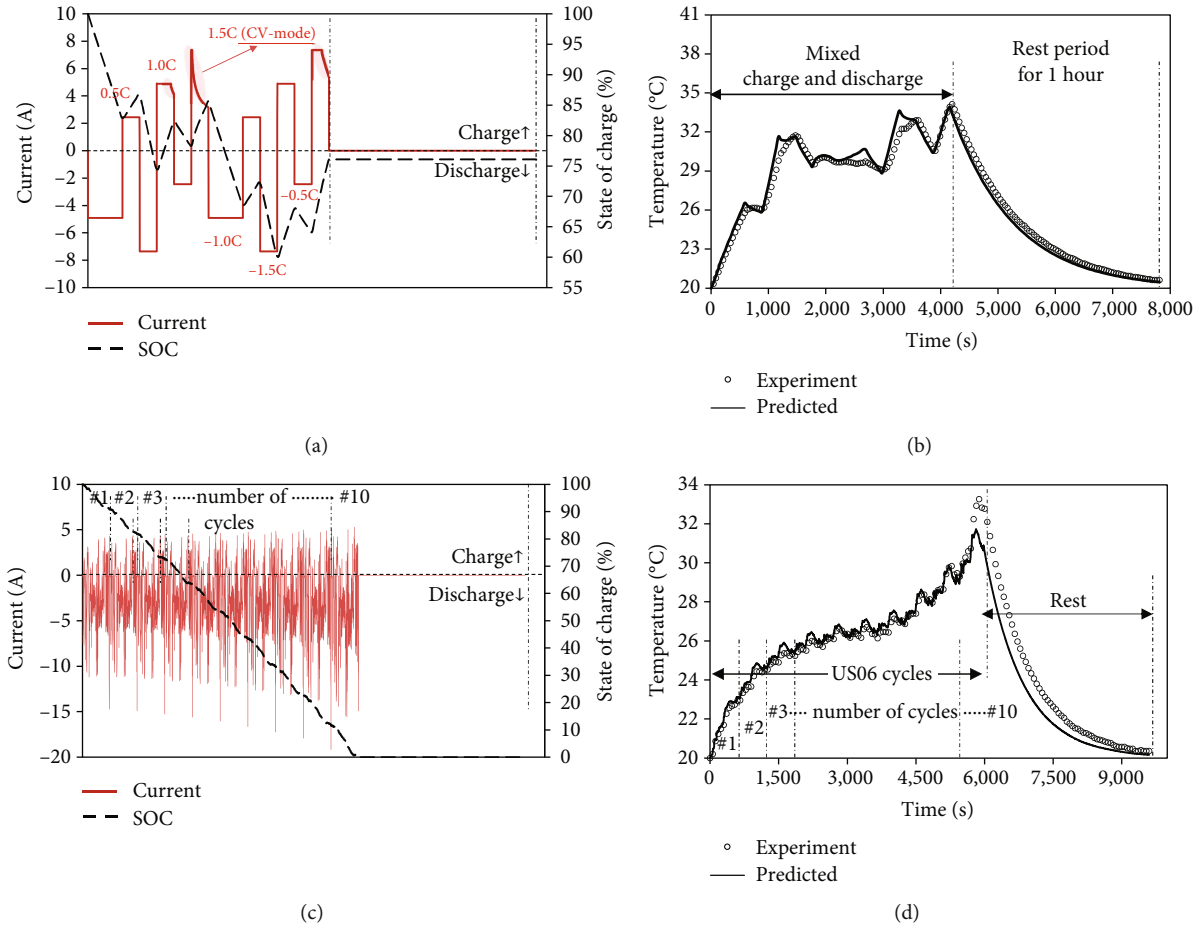

Figure 11: Validation under dynamic load conditions: artificially created cycle in the views of (a) current and state of charge and (b) battery temperature and US06 driving cycle in the views of (c) current and state of charge and (d) battery temperature [39].

discharging current are opposite, in which the sign of the charging current is set as positive in the current study, while it is set as negative in reverse. Considering this in terms of battery heat generation, since joule heat is proportional to the square of the current, it is always exothermic regardless of the sign of the current. In contrast, as the entropic heat is proportional to the current, thus it can be exothermic or endothermic depending on its sign.

To further clarify the phenomenon of entropic heat, the calculated entropic heat is shown in Figure 10(c), and it is so obvious that completely different trends of the entropic heat are generated during the operation. At the early SOC range below 40% the exothermal entropic heat is mainly generated for the discharging process, but the endothermal heat is generated for the charging process. At the middle ranges of 40% to 60% SOC, where the ECs are close to zero, it can be the entropic heat generation is nearly zero. Although less than in the early SOC range, exothermic and endothermic processes occur in opposite tendencies likewise at the final SOC range over 60%.

4.3.3. Dynamic Load Conditions. Thus far, the analysis has been conducted under constant C-rate, but nearly all battery systems, for instance, energy storage systems, EVs, and even portable electronic devices are actually operated in dynamic load conditions where the battery SOC varies up and down. Therefore, it is necessary to check whether the obtained ECs are valid in dynamic load conditions as well. For this reason, two types of dynamic operating cycles composed of both charging and discharging processes are prepared to investigate the effects of dynamic loads on the battery; one is an artificially created cycle, in which several charging and discharging C-rates are repeatedly performed, and the other is a dynamic current profile calculated according to the actual driving cycle of US06. To begin with the former, the applied current to the battery is determined, as shown in Figure 11(a), with the objective to linearly increase or decrease the battery SOC. The temperatures of the battery measured from the experiment and predicted using the obtained ECs are exhibited together in Figure 11(b), and the deviations between the experiment and simulation are shown to be less enough where the maximum RMSE is revealed to be 0.564°C.

For more dynamic loads conditions, the very complex current flows as shown in Figure 11(c) are applied to the battery, and accordingly, the battery SOC is changed every second. It is noted that the current profile of Figure 11(c) is obtained by referencing to the previous study [34], which

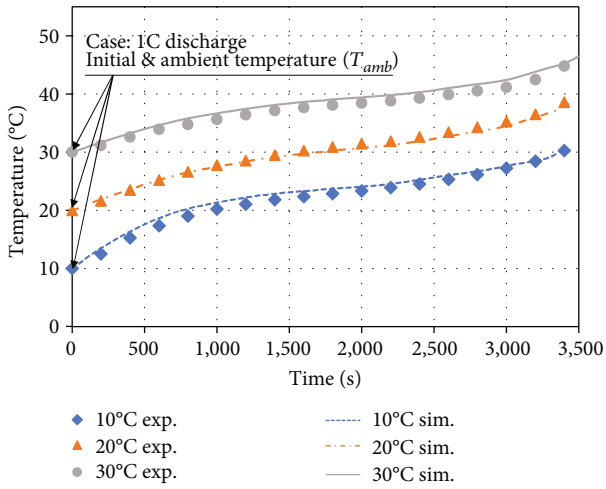

Figure 12: Validation for 1C discharge case under different 10°C to 30°C ambient temperatures.

investigates the dynamic loads of the battery. Similarly, the comparison results between experiment and simulation are indicated in Figure 11(d), and the maximum RMSE is recorded as 0.594°C either. From the results, the IHTA method is proven to be valid not only in the case where the SOC varies linearly but also in the case of very irregular variations, as shown in this section 4.4. However, it should be noted that the current study assumes there are no dynamic effects in the battery heat generation in the battery model development. From the literature review, it is noted that the extra heat, known as heat of mixing, can be generated in the case of dynamic operation in which the charging and discharging processes are mixed. This is due to the slow mass transport of lithium-ion between active materials and usually appeared to the electrochemical systems with bas or low transport properties, where the concentration gradients are limited [29]. In spite of this, the dynamic effect in the battery heat generation can be negligible for the high power battery applications, which are the same as the battery used in the current study. In addition, considering the ECs in the current study are obtained in constant C-rates with minor dynamic effect and presenting high precision in thermal prediction in two above dynamic cycles, the assumption of no or minor dynamic effect is fairly acceptable.

4.3.4. Ambient Temperatures. Ever since that LiBs are very sensitive to their operating temperature, the electrochemical reactions within the cell are influenced according to the ambient temperatures. Therefore, as a final verification, it is tested whether the newly obtained ECs are valid in predicting the battery temperatures at different ambient temperatures. In this regard, the additional verification performed is under different ambient temperatures of 10°C and 30°C for the case of 1C discharge, and the verification results are shown in Figure 12. From the comparison with the experimental values, the maximum RMSEs of simulation under different ambient temperatures are confirmed as 0.848°C. Although it is generally known that the battery is affected by the ambient temperatures because the different temperature increases are confirmed at different ambient temperature, ECs obtained from the IHTA method are likewise valid to precisely predict the battery temperature. As a result of validation from subsection 4.3.1 to 4.3.4, it is noted that the ECs obtained from the IHTA method can well predict the battery thermal behaviors over temperatures ranging from 10°C to 60°C.

5. Conclusions

In this paper, the high precision and time-efficient determination method to estimate the entropic coefficients of LiBs is proposed based on the inverse heat transfer analysis (IHTA) method. Through the step-by-step processes of IHTA method, the ECs are derived, and they are regressed based on least squares estimation to obtain the representative entropic coefficient as a function of state of charge. Through the comparison with the existing potentiometric method, the feasibility of the IHTA method is confirmed by showing same trends of the entropic coefficients according to the battery's SOC, and time efficient attributes are proven by reducing the experimental time over 93.7%. Last of all, the accuracy of the IHTA method is well validated by comparing the measured and predicted values on the battery thermal responses under various operating conditions. From the validation, the obtained entropic coefficients are realized to be satisfactory enough to predict the battery temperatures under different C-rates, charging process, dynamic load conditions, and different ambient temperatures. The accuracy of the proposed method is verified with the maximum RMSE of 0.848°C, and it is realized to be applicable to 10°C to 60°C temperature ranges.

To sum up, the proposed method could relieve the excessive experimental dependency of the existing method with the aid of the numerical approach, noticeably reducing the measurement time by simplifying the multistage experimental processes. Likewise, due to the extraction of continuous profiles of entropic coefficients, the accurate thermal prediction of the battery under diverse conditions is ensured. In this viewpoint, it is expected to be actively utilized in future battery thermal analysis.

Nomenclature

Symbols

A: area (m^2)
Bi: Biot number (-)
c: specific heat ($J \cdot kg^{-1} \cdot K^{-1}$)
C: capacity (Ah)
F: *Faraday constant*
h: heat transfer coefficient ($W \cdot m^{-2} \cdot K^{-1}$)
I: current (A)
k: thermal conductivity ($W \cdot m^{-1} \cdot K^{-1}$)
L: length (m)
m: mass (g)
n: number of electrons (-)
Q: heat (W)
t: time (s)

T: temperature (°C)
U: open-circuit voltage (V)
V: voltage (V)
ΔS: entropy change ($J \cdot mol^{-1} \cdot K^{-1}$)
y_i: experimental value
$\widehat{y}_i$: calculated value
η: operational efficiency (-)
∂R: overall uncertainty
δx_i: uncertainty of individual parameter.

Abbreviations

BTMS: battery thermal management system
CC: constant current
CC-CV: constant current-constant voltage
C-rate: current-rate [C]
CV: constant voltage
EC: entropic coefficient
EV: electric vehicle
exp.: experiment
GRG: generalized reduced gradient
GITT: galvanostatic intermittent titration technique
IHTA: inverse heat transfer analysis
LiBs: lithium-ion batteries
NCA: nickel cobalt aluminum
MSE: mean square error
OCV: open-circuit voltage
PM: potentiometric method
R^2: r-square
RMSE: root mean square error
sim.: simulation
SOC: state of charge
SSE: sum square error.

Subscripts

amb: ambient
c: characteristic
cell: battery cell
dis: dissipation
exp: experimental
gen: (heat) generation
irr: irreversible
oc: open-circuit
ohm: ohmic
non-ohm: non-ohmic
r: radial
rated: rated (nominal)
rev: reversible
z: axial.

Data Availability

Data will be made available as requested.

Conflicts of Interest

The authors declare that they have no conflicts of interest.

Acknowledgments

This research was supported by the program of the National Research Foundation of Korea (NRF-2019R1C1C1011195).

References

[1] S. Ma, M. Jiang, P. Tao et al., "Temperature effect and thermal impact in lithium-ion batteries: a review," *Progress in Natural Science: Materials International*, vol. 28, no. 6, pp. 653–666, 2018.

[2] C. She, L. Zhang, Z. Wang, F. Sun, P. Liu, and C. Song, "Battery state of health estimation based on incremental capacity analysis method: Synthesizing from cell-level test to real-world application," *IEEE Journal of Emerging and Selected Topics in Power Electronics*, vol. 6777, pp. 1–10, 2022.

[3] D. Li, P. Liu, Z. Zhang et al., "Battery thermal runaway fault prognosis in electric vehicles based on abnormal heat generation and deep learning algorithms," *IEEE Transactions on Power Electronics*, vol. 37, no. 7, pp. 8513–8525, 2022.

[4] A. R. Bais, D. G. Subhedhar, N. C. Joshi, and S. Panchal, "Numerical investigation on thermal management system for lithium ion battery using phase change material," *Materials Today: Proceedings*, vol. 66, pp. 1726–1733, 2022.

[5] Y. Wang, D. Dan, Y. Zhang et al., "A novel heat dissipation structure based on flat heat pipe for battery thermal management system," *International Journal of Energy Research*, vol. 46, no. 11, pp. 15961–15980, 2022.

[6] D. Bernardi, E. Pawlikowski, and J. Newman, "General energy balance for battery systems," *Journal of the electrochemical society*, vol. 84–2, pp. 164-165, 1985.

[7] H. Liu, Z. Wei, W. He, and J. Zhao, "Thermal issues about Li-ion batteries and recent progress in battery thermal management systems: a review," *Energy Conversion and Management*, vol. 150, pp. 304–330, 2017.

[8] X. F. Zhang, Y. Zhao, Y. Patel et al., "Potentiometric measurement of entropy change for lithium batteries," *Physical Chemistry Chemical Physics*, vol. 19, no. 15, pp. 9833–9842, 2017.

[9] K. E. Thomas, C. Bogatu, and J. Newman, "Measurement of the entropy of reaction as a function of state of charge in doped and undoped lithium manganese oxide," *Journal of the Electrochemical Society*, vol. 148, no. 6, p. A570, 2001.

[10] A. H. Thompson, "Thermodynamics of Li intercalation batteries: Entropy measurements on Li_xTiS_2," *Physica B+ C*, vol. 105, no. 1-3, pp. 461–465, 1981.

[11] J. Hong, H. Maleki, S. Al Hallaj, L. Redey, and J. R. Selman, "Electrochemical-calorimetric studies of lithium-ion cells," *Journal of the Electrochemical Society*, vol. 145, no. 5, pp. 1489–1501, 1998.

[12] A. Eddahech, O. Briat, and J. M. Vinassa, "Lithium-ion battery heat generation investigation based on calorimetric entropy measurements," in *2013 IEEE International Symposium on Industrial Electronics*, Taipei, Taiwan, 2013.

[13] M. Xiao and S. Y. Choe, "Theoretical and experimental analysis of heat generations of a pouch type $LiMn_2O_4$/carbon high power Li- polymer battery," *Journal of Power Sources*, vol. 241, pp. 46–55, 2013.

[14] K. Chen, G. Unsworth, and X. Li, "Measurements of heat generation in prismatic Li-ion batteries," *Journal of Power Sources*, vol. 261, pp. 28–37, 2014.

[15] Z. Geng, J. Groot, and T. Thiringer, "A time- and cost-effective method for entropic coefficient determination of a large commercial battery cell," *IEEE Transactions on Transportation Electrification*, vol. 6, no. 1, pp. 257–266, 2020.

[16] J. P. Schmidt, A. Weber, and E. Ivers-Tiffée, "A novel and precise measuring method for the entropy of lithium-ion cells: Δs via electrothermal impedance spectroscopy," *Electrochimica Acta*, vol. 137, pp. 311–319, 2014.

[17] P. J. Osswald, M. Del Rosario, J. Garche, A. Jossen, and H. E. Hoster, "Fast and accurate measurement of entropy profiles of commercial lithium-ion cells," *Electrochimica Acta*, vol. 177, pp. 270–276, 2015.

[18] N. Damay, C. Forgez, M. P. Bichat, and G. Friedrich, "A method for the fast estimation of a battery entropy-variation high- resolution curve - application on a commercial $LiFePO_4$/graphite cell," *Journal of Power Sources*, vol. 332, pp. 149–153, 2016.

[19] F. Geifes, C. Bolsinger, P. Mielcarek, and K. P. Birke, "Determination of the entropic heat coefficient in a simple electrothermal lithium-ion cell model with pulse relaxation measurements and least squares algorithm," *Journal of Power Sources*, vol. 419, pp. 148–154, 2019.

[20] Y. Hu, S. Y. Choe, and T. R. Garrick, "Hybridized time-frequency method for the measurement of entropy coefficient of lithium-ion battery," *Electrochimica Acta*, vol. 362, p. 137124, 2020.

[21] Y. Hu and S. Y. Choe, "Simultaneous and continuous characterization of reversible and irreversible heat of lithium-ion battery using wavelet transform technique," *Electrochimica Acta*, vol. 375, p. 137973, 2021.

[22] A. Abbasalinejad, M. M. Besli, J. W. Hammond, S. H. Chung, J. Christensen, and S. U. Kim, "Evaluation of the entropy of reaction using modified frequency-domain method and a physics-based thermoelectrochemical model of a lithium-ion battery," *Journal of Power Sources*, vol. 508, article 230283, 2021.

[23] H. R. B. Orlande, "Inverse heat transfer problems," *Heat Transfer Engineering*, vol. 32, no. 9, pp. 715–717, 2011.

[24] M. Guo, G. Sikha, and R. E. White, "Single-particle model for a lithium-ion cell: thermal behavior," *Journal of the Electrochemical Society*, vol. 158, no. 2, p. A122, 2011.

[25] L. Sheng, H. Zhang, L. Su et al., "Effect analysis on thermal profile management of a cylindrical lithium-ion battery utilizing a cellular liquid cooling jacket," *Energy*, vol. 220, article 119725, 2021.

[26] T. L. Bergman, F. P. Incropera, D. P. DeWitt, and A. S. Lavine, *Fundamentals of Heat and Mass Transfer*, John Wiley & Sons, 7th ed. edition, 2011.

[27] S. He, B. T. Habte, and F. Jiang, "LBM prediction of effective thermal conductivity of lithium-ion battery graphite anode," *International Communications in Heat and Mass Transfer*, vol. 82, pp. 1–8, 2017.

[28] G. Liu, M. Ouyang, L. Lu, J. Li, and X. Han, "Analysis of the heat generation of lithium-ion battery during charging and discharging considering different influencing factors," *Journal of Thermal Analysis and Calorimetry*, vol. 116, no. 2, pp. 1001–1010, 2014.

[29] C. Forgez, D. Vinh Do, G. Friedrich, M. Morcrette, and C. Delacourt, "Thermal modeling of a cylindrical $LiFePO_4$/graphite lithium-ion battery," *Journal of Power Sources*, vol. 195, no. 9, pp. 2961–2968, 2010.

[30] L. S. Lasdon, A. D. Waren, A. Jain, and M. Ratner, "Design and testing of a generalized reduced gradient code for nonlinear programming," *ACM Transactions on Mathematical Software*, vol. 4, no. 1, pp. 34–50, 1978.

[31] P. Y. Papalambros and D. J. Wilde, *Principles of Optimal Design: Modeling and Computation*, Cambridge university press, 3rd ed edition, 2010.

[32] G. Kemmer and S. Keller, "Nonlinear least-squares data fitting in excel spreadsheets," *Nature Protocols*, vol. 5, no. 2, pp. 267–281, 2010.

[33] M. Murnane and A. Ghazel, "A Closer Look at State of Charge (SOC) and State of Health (SOH) Estimation Techniques for Batteries," 2017. https://www.semanticscholar.org/paper/A-Closer-Look-at-State-of-Charge-(-SOC-)-and-State-Murnane-Ghazel/964c93c82bf2ee272c6491b3cb85a06529e935d2.

[34] U. Han, H. Kang, J. Song, J. Oh, and H. Lee, "Development of dynamic battery thermal model integrated with driving cycles for EV applications," *Energy Conversion and Management*, vol. 250, article 114882, 2021.

[35] S. Sdi, "Specification of product INR21700-50G," possible at https://www.ancoo-battery.com/en/product/INR21700-50G.html (2022.11.08), 2018.

[36] J. S. Horner, G. Whang, D. S. Ashby et al., "Electrochemical modeling of GITT measurements for improved solid-state diffusion coefficient evaluation," *ACS Applied Energy Materials*, vol. 4, no. 10, pp. 11460–11469, 2021.

[37] M. Akbarzadeh, T. Kalogiannis, J. Jaguemont et al., "Thermal modeling of a high-energy prismatic lithium-ion battery cell and module based on a new thermal characterization methodology," *Journal of Energy Storage*, vol. 32, article 101707, 2020.

[38] R. Fan, C. Zhang, Y. Wang et al., "Numerical study on the effects of battery heating in cold climate," *Journal of Energy Storage*, vol. 26, article 100969, 2019.

[39] U. Han, *Estimation of Reversible Entropic Heat of Lithium Battery Based on Inverse Heat Transfer Analysis and Least-Squares Optimization*, Purdue University, 2022.

[40] I. The Math Works, Curve Fitting Toolbox ™ User' s Guide R 2015 a, (2015) 754.

[41] V. V. Viswanathan, D. Choi, D. Wang et al., "Effect of entropy change of lithium intercalation in cathodes and anodes on Li-ion battery thermal management," *Journal of Power Sources*, vol. 195, no. 11, pp. 3720–3729, 2010.

[42] Y. Abdul-Quadir, T. Laurila, J. Karppinen et al., "Heat generation in high power prismatic Li-ion battery cell with LiMnNiCoO2 cathode material," *International Journal of Energy Research*, vol. 38, no. 11, pp. 1424–1437, 2014.

[43] A. Eddahech, O. Briat, and J. M. Vinassa, "Thermal characterization of a high-power lithium-ion battery: potentiometric and calorimetric measurement of entropy changes," *Energy*, vol. 61, pp. 432–439, 2013.